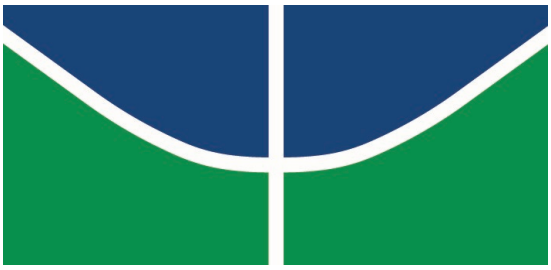

Universidade de Brasília

Instituto de Física

Master Thesis

Lightning Radio Pulses Amplitude and Altitude Relations as Observed by LOFAR

João Gabriel Oliveira Machado

Advisor: Prof. Luiz Roncaratti

Co-advisor: Prof. Ivan Soares Ferreira

João Gabriel Oliveira Machado

Relações de amplitude e altitude em pulsos de rádio emitidos por raios observados pelo LOFAR

Tese requerida para obtenção do título de mestre em Fìsica pelo Instituto de Física da Universidade de Brasília

Orientador: Prof. Luiz Roncaratti

Co-orientador: Prof. Ivan Soares Ferreira

Brasília, agosto de 2021.

Abstract

When a lightning flash is propagating in the atmosphere it is known that the negative leaders emit a large number of Very High Frequency (VHF) radio pulses. It is thought that this is due to streamer activity at the tip of the growing negative leader. In this work is presented a brief description of relevant lightning aspects and phenomena, as well a discussion regarding its radiation emission. Details from the mapping procedure using the LOFAR radio telescope, including data filtering, calibration, correction factors and pulse analysis are also discussed. Following these preliminary topics, it is investigated the dependence of the strength of this VHF emission on the altitude of such emission for two lightning flashes as observed by the LOFAR. It is found for these two flashes that the extracted amplitude distributions are consistent with a power-law, and that the amplitude of the radio emissions decreases very strongly with source altitude, by more than a factor of two from one kilometer altitude up to five kilometers altitude. In addition, any dependence on the extracted power-law with altitude is found, and the extracted power-law slope has an average around three, for both flashes.

Resumo

Quando uma descarga elétrica se propaga pela atmosfera é notório que líderes negativos emitem uma grande quantidade de pulsos de rádio VHF (Very High Frequency). Se acredita que essa emissão se dá pela atividade de *streamers* na extremidade de um líder negativo em seu desenvolvimento. Neste trabalho é apresentada uma breve descrição de aspectos e fenômenos relevantes às descargas elétricas, assim como discussão relevante sobre sua emissão de radiação. Detalhes do procedimento de imageamento com o telescópio em rádio LOFAR, incluindo filtragem de dados, calibragem, fatores de correção e análise de pulsos também são discutidos. Sucedendo estes tópicos preliminares, nós investigamos a dependência da amplitude dessa emissão VHF na sua altitude, para duas descargas elétricas observadas pelo LOFAR. Para estas duas descargas elétricas, é mostrado que as distribuições de amplitude extraídas são consistentes com uma lei de potência, e que a amplitude dos sinais de rádio emitidos decresce fortemente com a altitude das respectivas fontes, por um fator maior que dois entre cerca de um kilômetro e cinco kilômetros de altitude. Adicionalmente, é encontrada uma dependência da lei de potência obtida com a altitude de sua emissão, e que o coeficiente desta lei de potência possui valor médio de três, para ambas descargas elétricas.

Resumo expandido

Baseando-se em estudos anteriores feitos acerca das propriedades da amplitude de sinais de rádio emitidos por descargas elétricas, este trabalho mostra como se dá a relação entre a amplitude dos sinais emitidos por líderes negativos de descargas elétricas e sua respectiva altitude de emissão. Através da análise da radiação VHF emitida por líderes negativos de descargas elétricas por meio do rádio telescópio LOFAR, é possível relacionar a amplitude destas emissões em rádio com a altura em que são emitidas, consequentemente relacionando-a com a pressão do meio em questão.

Inicialmente, após a motivação inicial e breve descrição da tecnologia utilizada, é apresentado um resumo de fenômenos e características importantes acerca da física de descargas elétricas, como o desenvolvimento de líderes, a importância de streamers e do processo de *stepped leader*, e toda a nomenclatura utilizada ao longo do texto. Então é abordada em detalhes a questão da emissão de radiação, em específico radiação em VHF, e como ela pode ser detectada e mensurada. A partir destes conceitos então é apresentado o LOFAR. Sua grande capacidade de resolução espacial e temporal o tornam essencial para a detalhada análise requerida por este estudo.

Com base nos conceitos apresentados, é introduzido o processo de tratamento de dados necessário para a apropriada visualização e análise dos dados obtidos de descargas elétricas, também con-

hecido como mapeamento. Por meio deste é possível visualizar o ponto de emissão do sinal de rádio detectado com resoluções de até dez metros e dez nanosegundos, algo atingido somente pelo LOFAR até então. Esta precisão permite visualizar os *bursts* de emissão em rádio, assim como sua amplitude de emissão. Após a devida apresentação dos fatores de correção necessários para avaliação dos resultados obtidos, algo que envolve correções para função de antena, consideração dos ângulos de emissão da radiação e também interferência no sinal, os resultados são apresentados.

Através de distribuições das amplitudes de emissão dos sinais detectados e de sua dependência na altitude do sinal emitido é possível ver uma relação de lei de potência entre os dois. Tal relação se dá de forma oposta ao esperado, baseando-se em estudos conduzidos em ambientes controlados de laboratório. Para estas duas descargas elétricas, é mostrado que as distribuições de amplitude extraídas são consistentes com uma lei de potência, e que a amplitude dos sinais de rádio emitidos decresce fortemente com a altitude das respectivas fontes, por um fator maior que dois entre cerca de um kilômetro e cinco kilômetros de altitude. Adicionalmente, é encontrada uma dependência da lei de potência obtida com a altitude de sua emissão, e que o coeficiente desta lei de potência possui valor médio de três, para ambas descargas elétricas.

CONTENTS

CHAPTER 1

INTRODUCTION

1.1 Motivation

Even though atmospheric lightning is a vastly known phenomena throughout the whole world, many aspects of its phenomena are not quite understood, nor the precise behaviour of its various properties. Its incidence, regardless taking place usually among storms, varies greatly in time, place and duration all over the globe, the only common factor among them being the randomness of its origination and behaviour [1]. Over a century of detailed works on lightning study and measurements was able to form a rather complete set of its related phenomenology, but this has not been the case for its physical understanding.

It is thought that VHF (30-300 MHz) radio emission from lightning is dominated by streamer activity [2, 3, 4, 5], from both positive and negative leaders, where a streamer is a self-propagating structure which develops inside a charged region, and a corona is a region of very weakly conducting plasma around a leader, generally thought to consist of many streamers [6]. From laboratory experiments [7, 8] it is known that the streamer activity depends strongly

on air density, in particular [9, 10] have shown that streamer propagation speed increases with decreasing air density. Following these works it is natural to expect that the amplitude of VHF radio emission from lightning should vary with pressure. Since streamers can be thought of as a moving head of charge, the VHF emission should be roughly proportional to the charge of the streamer times its acceleration. Since the velocity of a streamer increases with decreasing density, the acceleration should increase as well, thus it may be reasonable to expect that the VHF emission from lightning should increase at higher altitudes. However, alternatively, in the laboratory experiments of [8] it is shown that the amplitude of the corona current pulse decreases less than linear with decreasing air pressure, while the width of the current pulse increases much faster than linear when keeping the same ratio between applied voltage and onset voltage [fig 6, [8]]. This implies that the time-derivative of the corona current, and thus the VHF emission, should strongly decrease with altitude, in sharp contrast to the previously suggested model, where this relation is directly proportional.

Previous works have used lightning mapping arrays to investigate the distribution of VHF amplitudes from lightning flashes [11, 12, 8]. These studies have found that possibly larger flashes could emit stronger VHF amplitudes. However, they did not explicitly explore the dependence of VHF amplitude with altitude. In this work it is explored the distribution of VHF emission vs altitude from negative leaders from two lightning flashes. LOFAR's unique ability to store the entire raw waveform of the lightning flash for later processing is exceptional in order to ensure that the results are not affected by imaging artifacts.

1.2 Objectives

The investigation of the density (or equivalently the altitude) dependence of VHF emission from streamers is indicative of the basic physics behind the lightning corona, although the detailed relationship is not understood. Therefore, following the work of [13, 3, 14], this work analyses the data from two different flashes, from different dates, detected by LOFAR.

The main objective of this work is to investigate the amplitude dependence on the altitude of VHF signals emitted by negative lightning leaders of both flashes. This is done by a thorough process of data analysis and correction factors described in chapter 3.

As explained in chapter 4, up to the altitude of six kilometers, where the pressure is roughly half the pressure at ground level, it is demonstrated that for both analysed flashes the strength of the top 10% pulses decreases by a factor of three. This strongly implies that the amplitude distribution follows a power law, which is scale invariant.

1.3 Equipment and Technology

Even though lightning strikes occur quite frequently, averaging over 65 strikes per second (6 km^{-1} yr^{-1}) over the whole earth [6], its detailed detection is an onerous work and requires an enormous amount of both speed and precision capability from equipment as well as increasingly improving algorithms for processing this data. Ranging from portable devices used in aircraft-based measurements to large arrays comprised of several antennas, direct lightning detection can be based upon its electric field measurement or radio and optical emission detection. The use of antenna and telescopes arrays is by far the most advanced employed mean

of detection, and it is the one used in this work.

The Low-Frequency Array, or simply LOFAR, is a high precision radio telescope capable of surveying the low-frequency radio sky, detecting cosmic-rays, measuring cosmic magnetism and other relevant aspects for astronomical sciences. The interest in it is in the fact that it can locate lightning VHF sources quite precisely, with temporal and spatial resolution of 10 ns and 10 meters, respectively. It consists of over 4512 low-band antennas and 2256 high-band antennas distributed within dozens of stations scattered across The northern Netherlands and a few other stations in different European countries, but the high-band antennas are not used for mapping lightning. For lightning observations the low-band antennas operating over the $10 \sim 90$ MHz range are used [15]. LOFAR's huge advancement in lightning detection comes not only from its high temporal and spatial resolution, but also the fact that its low noise level makes it possible to detect many more pulses than any other antenna array, such as a LMA (Lightning Millimeter Arrays), and view in detail negative leaders stepping process, lightning needles and individual pulses [13, 3].

Figure 1.1 shows a typical lightning VHF pulse as detected by LOFAR [16]. These pulses are extremely similar to the impulse response function of the LOFAR antennas, and thus the frequency spectrum is fairly flat in LOFAR's frequency band. Therefore, any attempt to extract information from the frequency spectra would need to explore very subtle effects and would be prone to instrumental artifacts, requiring first the entire processing of the raw data. This processing is comprised of calibrating the antennas signal, mitigating radio-frequency interference (mainly from human-generated sources) and other small amplitude noises, and finally cross-correlating the data in a iterative interferometric method. This processing and data analy-

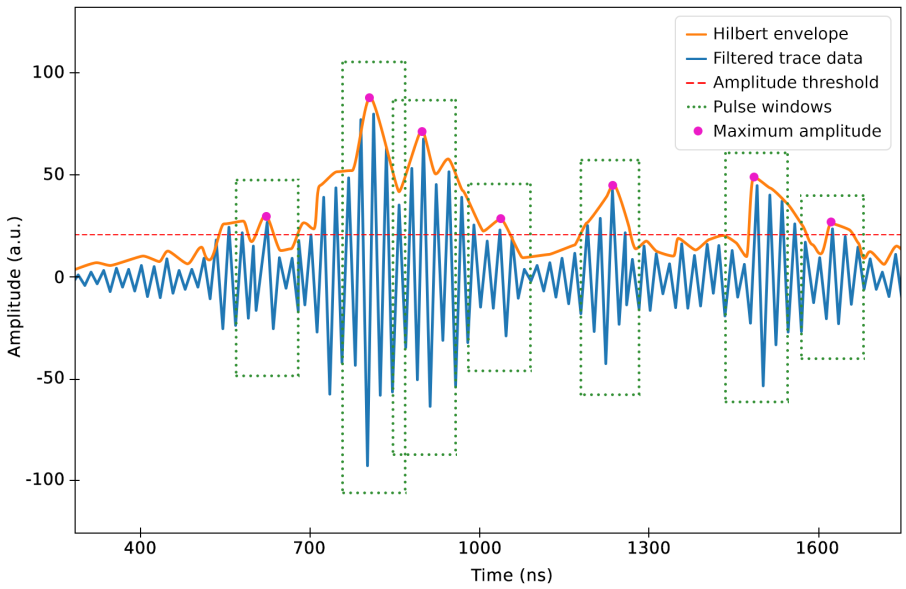

Figure 1.1: A filtered trace from the data with its Hilbert envelope. The dotted green line depicts the windows for the pulse detection algorithm, which are 10 samples wide, and the pink points show the peak amplitudes inside each window. The threshold for pulse detection is set at an amplitude of 15 which is about 3 standard deviations from the noise baseline. Amplitude is given in arbitrary units.

sis is further detailed in chapter 3 and the necessary correction factors for the raw data acquired by LOFAR are discussed in detail on sub-chapter 3.3.

CHAPTER 2

THE PHYSICS OF LIGHTNING

Lightning is an intricate and vast research field, many times connected with alike fields such as earth atmosphere and cosmic rays, and many are the cases in which authors have named and categorized different discovered phenomenology in distinct manners, and there are such cases in which the same term is used for two unlike phenomena or mechanisms by different authors. First it is required a brief description of such phenomenology and the introduction of the correct terminology that is used along this work, and this chapter covers this need.

2.1 General Factors

Since lightning is characterized by a quite distinguished, bright and fast optical flash it is necessary to start with the very definition of a lightning flash, which is precisely the lightning discharge that arises within clouds and develops towards the ground, reaching it (cloud-to-ground or CG flash) or not (intra-cloud or IC flash). The very initiation mechanism of a lightning

flash is not yet quite understood, but recent studies provide a great insight into this complex matter [17]. This flash can reach over several kilometers in extension and it is electrical in its nature [6], where it is possible to make another phenomenological distinction: its electrical charge. The several "branches" of a lightning which are formed as it propagates through the atmosphere are the positive and negative leaders, a self-propagating discharge that creates an electrically conductive space behind its propagation path, and this distinction between them is important since they entire development mechanism differs from one to the other.

A negative leader, which is the one analysed throughout this work, is the most common initiation leader of a cloud-to-ground flash [6]. A leader, being it positive of negative, is comprised of many small self-propagating discharges called streamers, that unlike a leader, creates an insulating space behind its propagation path. These structures are the foundation of a negative leader development, which is a rather inconspicuous mechanism called stepping process. Several models were made in attempt to fit what is observed and measured [18, 19, 20, 21, 22] until a broadly accepted model that fits obtainable data has been proposed and further refined, depicted in figure 2.1.

This stepping process, as the name implies, consists of repeating steps where in each step a burst of streamers arise from the very tip of the leader propagation path creating what is called a space stem, a very optically-bright occurrence on the very end of the streamer region. Streamers of both polarizations are created within this space stem, developing in opposite directions from one another. The positive ones towards the negative leader tip and the negative ones in the opposite direction. When enough current exists within this space stem, it is transformed into a space leader, developing towards the very tip of the negative leader. When these two

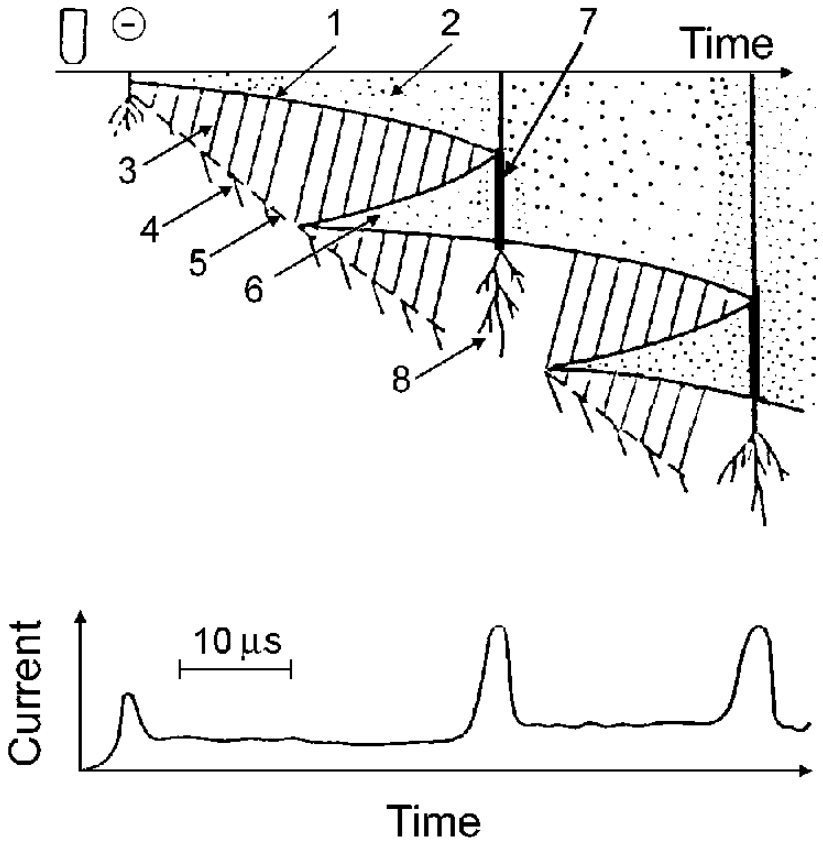

Figure 2.1: Illustration of a mechanism of the negative stepped leader in a long laboratory spark. The negative electrode is seen at the left of the figure. 1, leader tip; 2, primary leader channel; 3, positive streamers of the streamer zone; 4, negative streamers of the streamer zone; 5, space stem; 6, secondary channel; 7, leader step; 8, burst of negative streamers. Adapted from [23], extracted from [24]

leaders reach one another, a very bright flash is seen along the whole space leader path, creating a burst of streamers that repeats the entire described process until enough energy is dissipated and the further transformation of space stems into space leaders is no longer possible [25]. The stepping process for negative leaders differs from the stepping process for positive leaders [26].

Corona discharges (not to be mistaken with the corona region of a discharge)[27], runaway electrons[28] and other luminous events such as halos, sprites and elves are also artifact produced by lightning phenomena [29, 30], but these lay outside the scope of this work.

The very first electromagnetic signals detected from a lightning strike occur before the lightning itself starts propagating comprises the initial breakdown[31], which for IC flashes are longer signals emitted as the leader is still covering the gap between the opposite charged regions of the cloud and for CG flashes are easily distinguished signals originating inside a cloud. These early pulses behave differently from the ones emitted as a leader is developing and are characterized mostly by its bipolar nature and mean duration of 780 μs[32].

2.2 Radiation Emission and Detection

Since lightning is a complex phenomena with many individual electromagnetic processes structuring it, it is naturally expected that radiation arises from it. Ranging from as low as 1Hz frequencies, lightning radiation has been measured all over the electromagnetic spectrum [6], with secondary phenomena reaching as high as gamma-ray energies [33]. These high-energy events are generated by runaway electrons, terrestrial gamma-ray flashes and other high-energy events which lay outside the scope of this work.

Through the stepping process of negative leaders propagation, several VHF pulses are emitted [3]. This emission happens not once per step, but a burst of short, discreet VHF pulses is emitted by what shall be called a source. Following laboratory experiments, this emission is thought to be associated with corona flashes [34, 35], which should take place as the streamers are created within the space stem in the stepping process. These pulses are optimally observed by radio detectors but require sufficiently advanced technology in order to precisely measure its properties.

The most common mean of measuring these signals is with the use of large telescope systems, gathered in what is called an array. These arrays are comprised of several antennas that detect these VHF pulses as they are produced, enabling the temporal and spatial reconstruction of every detected source by an interferometric method, such as the time-of-arrival (TOA) method or other techniques [1]. VHF Lightning Millimeter Arrays, or LMAs are optimally constructed for the observation of lightning-emitted radio pulses and the interferometric processing of such data, and serve as great probes of both IC and CG flashes VHF activity [6].

One such VHF Array is the Low-Frequency Array, or LOFAR, a high precision radio telescope capable of locating lightning VHF sources with meter and nanosecond precision. It consists of over 4512 low-band antennas and 2256 high-band antennas distributed within dozens of stations scattered across The northern Netherlands. There are also international stations in other European countries, but they are not used for mapping lightning. For lightning observations the low-band antennas operate over the 10$\sim$90 MHz range are used [15].

Figure 2.2: Aerial view of the small island consisting of Superterp, LOFAR's core, located near the village of Exloo, on northern Netherlands. Extracted from [15].

Each core station (figure 2.2) is comprised of 96 low-band antennas and 48 high-band antennas, each one individually recording data with a resolution of 5 ns on each of its polarities. This provides a resolution on the decameter and 10 nanosecond level for mapping purposes using the algorithm developed by [16], a great advance in the lightning mapping field.

The advantage in using LOFAR for this work relies in its great precision and resolution for negative pulses mapping where so far no other LMA, or any interferometric telescope array for that matter, was able to achieve such resolution and precision. Also, it has not yet been reported any study aiming to observe the relation between amplitude and altitude on negative leaders produced by lightning, this study being the first to do so.

CHAPTER 3

DATA ANALYSIS

Two lightning flashes are investigated in this work, one from 29 September 2017 at 17:34:55 UTC, and another from 13 August 2018 at 15:30:01 UTC, referred to as the “2017" and “2018" flashes respectively, that were detected by LOFAR and imaged as described in chapter 3.1. In order to investigate the effect of pressure on the VHF emission of lightning, negative leaders from these two flashes are selected, and the distribution of recorded pulse peak amplitudes at different altitudes with 500 m tall altitude bins is found. For the VHF sources located on negative leaders within a certain altitude range it is determined the distributions of peak amplitudes in a reference antenna. These distributions are analyzed in section 3.2.

3.1 Imaging with the LOFAR Radio Telescope

At this point it is important to make a distinction between the data before the interferometry (from now on denoted simply raw data) and after it goes through the interferometry

algorithms (from now on denoted simply imaged data). The raw data consists of several sinusoidal signal files with the whole raw radio signal captured by each of LOFAR's antennas for the duration of the lightning flash. Whereas the imaged data consists only of the mapped lightning flash, after all data processing. In other words, the raw data is submitted to noise filtering and after the antennas have been time-calibrated, a source finding algorithm does the job of cross-correlating every potential source and minimizing its RMS value for position and time (the entire data treatment and mapping procedure is thoroughly explained by Scholten et. al. [36]).

Regarding the processing of the raw data, RFI mitigation is needed in order to remove as much as possible human-generated radio interference. This RFI processing is done in data blocks of 2^{16} time samples long. For each block a half-Hann window is applied at its beginning and ending, and a Fourier transform takes place at every block to easily apply band-pass filters and further RFI attenuation processes, as described in detail by Hare et al. [16].

In order to find actual VHF pulses within the filtered data, an algorithm was created. It consists of a routine that goes through the entire filtered data looking the highest peak within 10 time samples threshold, and then selecting this peak as the amplitude of a source, as indicated in figure 1.1. The output of this algorithm thus consists of the raw data. Two exceptions are excluded from this selection: the first is the signal emitted by two very close sources, spatially or temporally, as their detected signal may be comprised of overlapping pulses that make this selection inaccurate; the second are small peaks, peaks that are below certain threshold, as discussed below.

The process for generating of the imaged data is far more complex as it also involves

interferometry for the locations of the sources. Since recent works went through the entire imaging process in detail [16, 3, 14], a rather simple account of the imaged data processing follows.

For the imaged data, it is necessary to apply the same data filtering to the data from all antennas, and the process is the same as the one for the raw data up to the pulse finding part. The next step is time calibrating the stations. This accounts for inaccuracies between different stations clocks, both core and remote ones, using a selected antenna as the reference one (usually from the center-most station). In this part a few selected pulses from the reference antenna are used for minimizing the calculated arrival times and measured arrival times on all antennas, by means of a chi-square fit that goes through an increasing radius around the reference antenna, each iteration accounting for farther antennas until all antennas have been calibrated. Pulses are found in a similar manner, but instead of using only a few selected pulses as in the calibration step, all pulses (following a quality criteria) on the reference antenna are cross-correlated with other antennas on a chi-square fit until their optimal location has been found, generating the imaged data ready for further criteria filtering and analysis.

Since it is much easier to filter out unwanted sources by their spatial and temporal visual selection (much like figure 3.1-A), the selection of negative sources is straightforward once the positive and negative leaders are identified. Return strokes are not accounted for in this analysis, as their development mechanism differs from the negative leaders development. Imaged source locations locations are depicted in figures 3.1 and 3.2, which shows the image of the 2017 and 2018 flashes, respectively, with the negative leaders used in this work indicated.

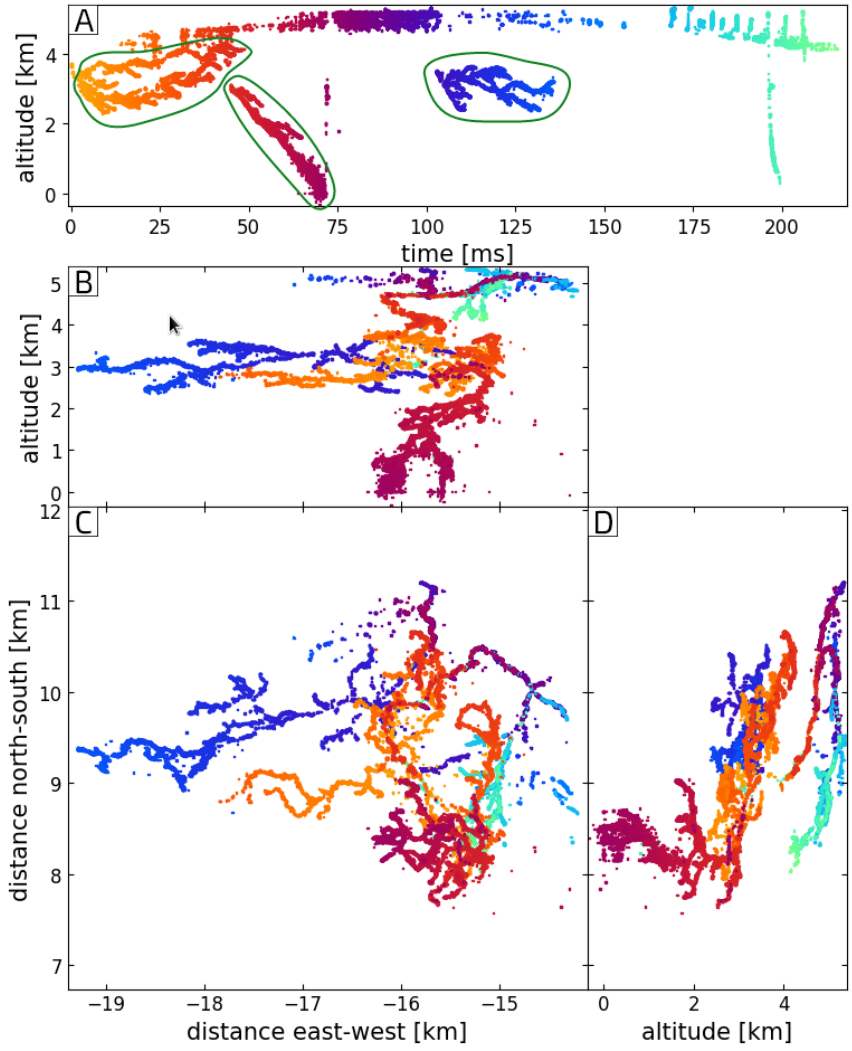

Figure 3.1: Plan view of the 2017 flash imaged data, coloured by time. Each point represents a located VHF source. Negative leaders are circled in green. A) Time vs altitude (from ground). B) east-west distance (from core center) vs altitude. C) east-west distance (from core center) vs north-south (from core center). D) altitude (from ground) vs east-west distance (from core center).

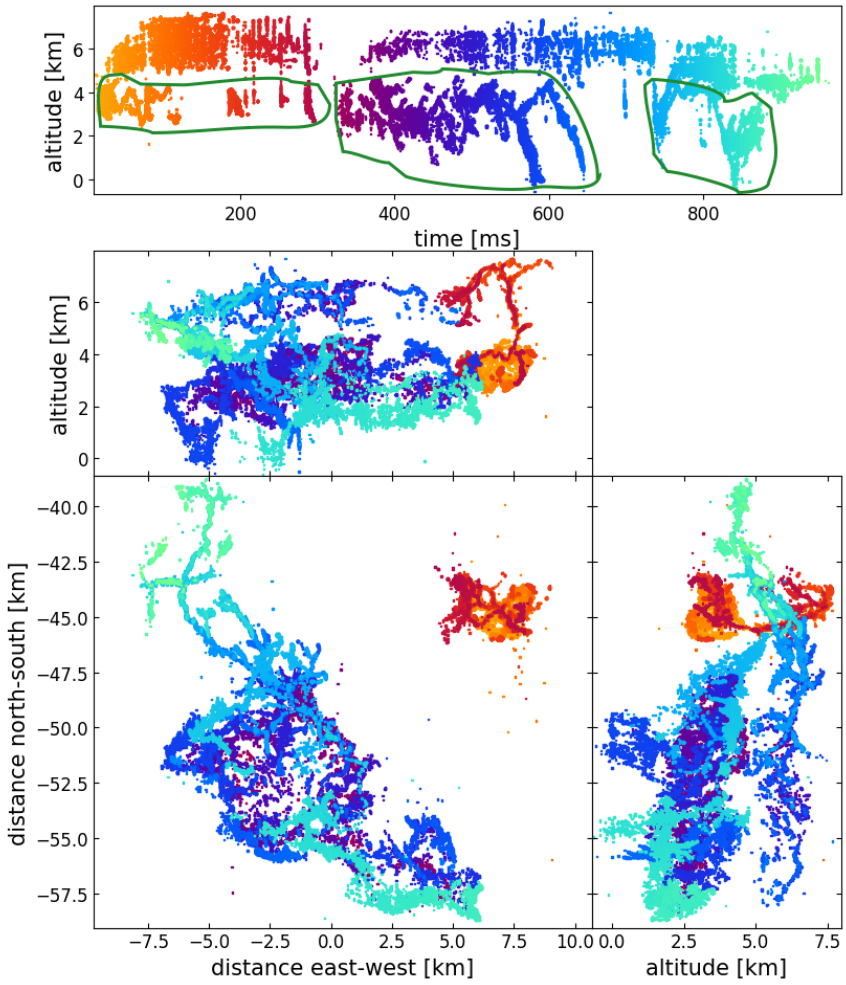

Figure 3.2: Plan view of the 2018 flash imaged data, coloured by time. Each point represents a located VHF source. Negative leaders are circled in green. A) Time vs altitude (from ground). B) east-west distance (from core center) vs altitude. C) east-west distance (from core center) vs north-south (from core center). D) altitude (from ground) vs east-west distance (from core center).

3.2 Analysis of Pulses

As demonstrated in figure 1.1, VHF radiation from lightning, as observed by LOFAR, is extremely impulsive, where each recorded pulse has a full-width-half-max (FWHM) of around 50 ns. As a proxy for the amplitude of each radio source, the peak amplitude of the pulse is taken as recorded by a central antenna, called the reference antenna. Since the only interest here is in how the amplitude changes with source altitude, any absolute calibration is performed, and only the amplitudes as measured by the digitizer are presented. The negative leaders from the two flashes considered in this work were arranged in 500 m tall altitude bins and for each bin the strength distribution of the sources is analyzed.

The efficiency of the used imaging algorithm depends on pulse strength, strong pulses clearly stick out and are thus more easily recognized than weaker ones. This potentially introduces a pulse-amplitude dependent bias. To explore this, figure 3.3 shows the amplitude spectrum of all received radio pulses between times t=100 ms and t=150 ms from the 2017 flash shown in figure 3.1, as well as the amplitude spectrum of the located sources in the same time period. The error bars indicate the statistical uncertainty and are therefore large for the top bins where the number of counts is small. This selection was chosen because there was very little activity elsewhere during this time, and because the negative leaders occurred over a relatively narrow altitude range. For most other cases this comparison cannot be made as there is lightning activity at many different altitudes and it is necessary to locate the source. As expected, the source locations could be found for almost all strong peaks and for the weaker ones the pulse-finding efficiency becomes gradually worse. This is also expressed in the lower panel

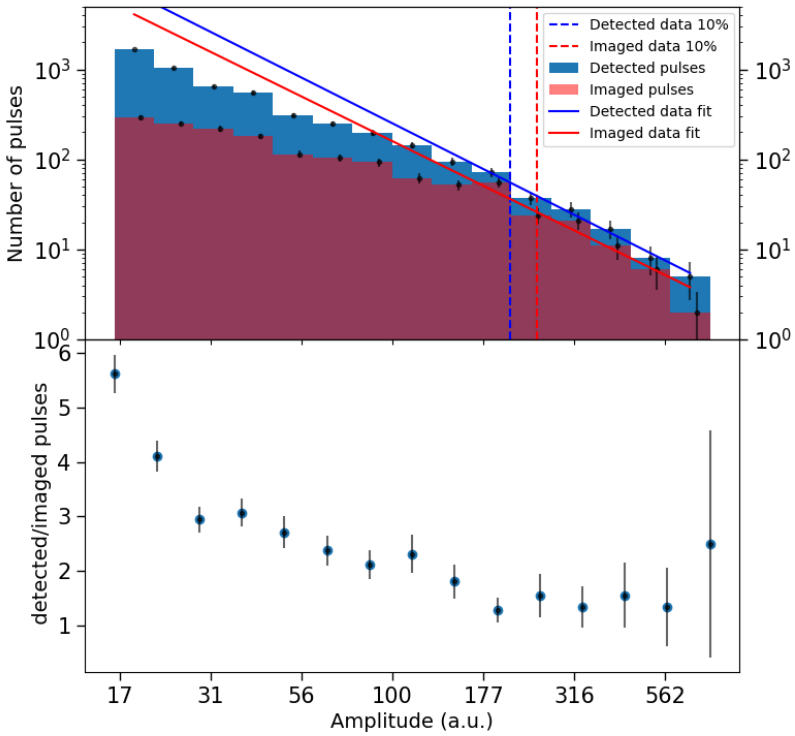

Figure 3.3: The upper image shows on a log-log scale an overlapping comparison between the distributions of amplitudes of located sources and all pulses as detected in the reference antenna between times t=100 ms and t=150 ms from the 2017 flash. The solid lines show a power-law fit to the strongest 10% of sources, and the vertical bar shows the 10% amplitude. The power-law slope, λ, for both fits is 2.32. The lower panel depicts the ratio of the number of located and all pulses per amplitude bin. Amplitude is in arbitrary units.

of figure 3.3, showing that the ratio between the two amplitude distributions (number of located divided by the number of all pulses) is fairly constant and close to unity for the strongest 10% pulses. This is also shown by the fact that fits to the strongest 10% pulses with a power-law (equation 3.1), a straight line on a log-log scale, as described later in this chapter, yield the same slopes for the two distributions. Therefore this work is focused on the strongest 10% of located pulses where the 10-percentile amplitude is indicated by the vertical dashed line in the figure.

To characterize the pulse distribution at large amplitudes two different statistics are explored. The absolute pulse strength is characterized by the 10-percentile amplitude. This

statistic was chosen because the maximum amplitude for a stochastic process will increase with the number of analyzed pulses while a percentile value is more stable. The 10% amplitude was chosen since this is the largest percentile that is not much affected by the imaging efficiency as seen from figure 3.3. The two vertical bars in figure 3.3 show the 10% cut amplitude for the imaged and all pulses. Due to the smaller imaging efficiency at smaller amplitudes the 10% value for all pulses is somewhat smaller than for the imaged sources. However, any expectation is made of significant influence of this effect in the obtained results, as a similar effect is observed on amplitude distributions for all analysed data. In addition it is also reported the slope λ of a power-law fitted to the strongest 10% of events,

$$N(a) = N_0 a^{-\lambda} \,, \tag{3.1}$$

where $N(a)$ is the number of events at amplitude a and N_0 is a normalization factor. A power-law was chosen instead of an exponential distribution as this yields a better fit to the data.

3.3 Correction Factors

There are several factors that affect the relation between the detected pulse amplitude and the actual emitted amplitude. Some of these will be important for the altitude dependence investigated in this work.

Since an impulsive source is likely driven by a rapidly changing current with a certain orientation, the VHF emission will have an angle-dependent emission pattern, likely similar to

dipole emission. This will potentially affect the detected strength. However, since the emission from many sources that are likely to have random orientations, the great majority of them are above the 2 km line, where the leaders are mostly horizontally-oriented, and as such, their emission should follow the same pattern. Even so, if all these emission were mostly vertically-oriented, this would incur a multiplicative factor on the final results, which would not change its interpretation significance, as explained in chapter 4.

Sources that are further away will have weaker recorded amplitudes in the reference antenna. This however, is not a significant concern as the spatial extent of each of the two flashes is much smaller than the distance to the flash itself ($\approx$ 18.6 km for 2017 flash and $\approx$ 50 km for the 2018 flash). Therefore, while the measured amplitudes cannot be compared between flashes, the shape of the amplitude distribution should be robust to distance variations within each lightning flash.

More importantly, however, are the effects of LOFAR's antenna function. Radio emission from different sources will arrive from different elevation (θ_e) and azimuth (ϕ) angles, and therefore will be amplified differently by the antenna function. The azimuth-angle dependence is not very strong as all sources are in a small angular regime where the antenna function is large. Particular care needs to be given to the elevation angle as the LOFAR antennas have vanishing sensitivity for sources at $\theta_e = 0$. Basic analytic considerations for the angular dependence of the measured amplitude one thus concludes that the antenna function is proportional to $\sin(\theta_e)$ for the small values of θ_e that are relevant for this work. Since $\sin(\theta_e) \approx \tan(\theta_e) = h/R$, where h is the altitude of the source and R the distance. One should correct for this linear altitude dependence to deduce the true altitude dependence of the source amplitude from the measured

amplitude. Further detailed description of LOFAR antennas functionality is given by [37].

CHAPTER 4

RESULTS

Table 4.1 show the results for the extracted statistics on the pulse distributions for the 2017 and 2018 flashes respectively. For each the altitude range, the number of located sources, the 10% percentile amplitude a_d, the same value corrected for the antenna function a_c, and the fitted power-law slope. As argued in chapter 3.3, the correction of the pulse strength is inversely proportional to the altitude of the source. Normalizing the correction to unity at 5 km gives:

$$a_c = \frac{5}{h} a_d \ , \tag{4.1}$$

where h is the mean altitude of the bin in units of km.

For these two flashes the presented data show that the a_d values tends to increase slowly with altitude, however when corrected for the antenna function, a_c, the values rapidly decrease with altitude as can be seen from figure 4.1. This shows that the peak amplitudes of individual

Table 4.1: The parameters for the amplitude distributions for negative leaders at different altitude sections for the two flashes considered in this work. The first column is the altitude range. For each flash the first gives the number of sources in the negative leader at that altitude, the second column gives the 10-percentile value of the measured amplitude (a_d), which is corrected for the effects of the antenna function in the third column (a_d), and the last column gives the the power-law slope, λ.

	2017 flash				2018 flash			
Altitude	sources	a_d	a_c	λ	sources	a_d	a_c	λ
0.0 - 0.5 km	353	137	2740	3.62	74	99	1980	4.64
0.5 - 1.0 km	1077	215	1433	2.42	110	93	620	2.50
1.0 - 1.5 km	910	255	1020	1.73	368	102	408	2.85
1.5 - 2.0 km	1643	292	834	2.45	721	116	331	4.03
2.0 - 2.5 km	1496	311	691	2.28	893	123	273	4.46
2.5 - 3.0 km	3714	312	567	2.90	1866	137	249	3.42
3.0 - 3.5 km	3110	322	795	2.93	2818	149	229	3.31
3.5 - 4.0 km	1709	324	432	2.11	3434	162	216	3.51
4.0 - 4.5 km	652	286	336	2.65	2048	166	195	2.48
4.5 - 5.0 km					429	200	210	1.82
5.0 - 5.5 km					25	156	148	1.05

VHF pulses decreases strongly with increasing altitude for these two flashes for leaders below 5 km altitude. These early results demonstrate the ability to explore the properties of VHF emission to much higher detail than possible before. Since these two flashes have a distinct development and occurred in different contexts (being observed a year apart), this implies that the observed strong amplitude fall-off with altitude could be general. This will be explored in future work. Previous studies [11], have suggested that flash size could impact the overall VHF magnitude of a lightning flash. Unfortunately, in this early work it proved unable to explore the difference in overall magnitude between the two lightning flashes. Since recent work [2, 3] has strongly suggested that VHF emission from lightning comes from streamers, The observed VHF peak amplitudes are indicative of lightning streamer amplitudes.

Since the analyzed negative leaders at lower altitudes are mostly vertical and the ones at higher altitudes are mostly horizontal, the fact that the streamer directions are not randomly

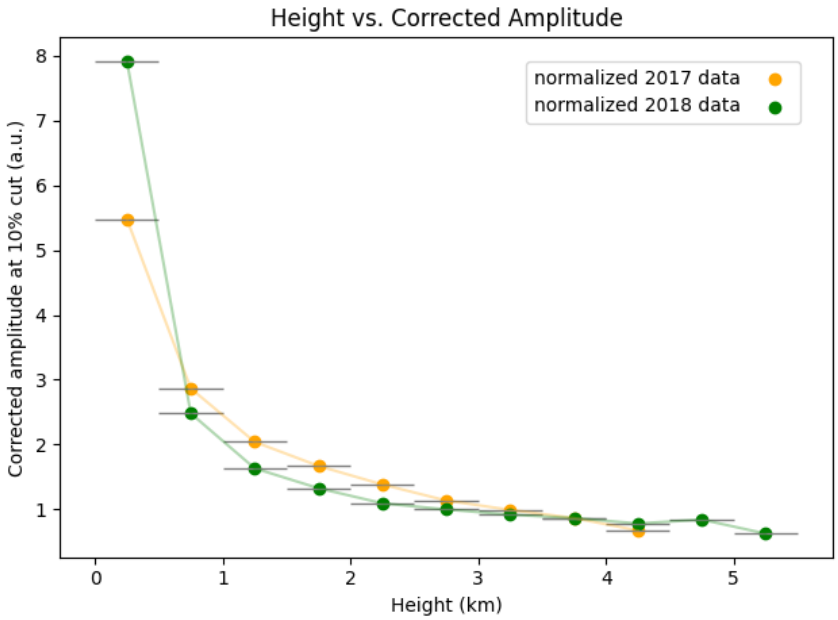

Figure 4.1: The altitude dependence of the corrected ten-percentile amplitudes (a_c from table 4.1) are shown for the two flashes. The values for the two flashes have been normalized to each other for the 2.5 – 3.0 km altitude bin. The vertical error bar indicates the bin size in altitude.

oriented as initially assumed may seem to be a problem, but if we consider an extreme scenario where the streamers close to ground are purely vertical and the streamers from the horizontal leaders in the cloud are random, then the average received amplitude should only differ by a factor of $\sqrt{2}$. However, the presented results show that the amplitude can change by a factor of five-eight from ground to cloud level. Thus, these results are too strong to be explained by a streamer distribution that is not oriented purely randomly as assumed in chapter 3.3.

CHAPTER 5

CONCLUSION

Previous results from laboratory streamer experiments [8, 12, 11] indicate that, for a fixed value of the electric field over breakdown, the current in a streamer decreases with decreasing pressure while at the same time also the width of the current pulse increases. Relating the medium pressure, in this case the air pressure, with the altitude in which the radiation emission takes place makes possible to expect the same reasoning in an natural lightning event, but this is not observed.

Figure 6 of [8] indicates that the pulse-width increases by about a factor of three when the pressure halves. Since the radiated power is expected to be proportional to the current-change, it is expected that the radiated power to decrease strongly with increasing altitude like is shown from the presented results. However, the strong increase of pulse strength towards lower altitudes appears not consistent with laboratory results and rather suggest that the proximity of the ground plays is important. It is important to stress the statistical reliability and

resolution provided by LOFAR, and also the fact that the amplitude for each pulse is computed individually, and not the emitted radiation as a whole.

Several possibilities arise for such case where there is a power-law inverse relation between the altitude and the amplitude, such as the Townsend scaling relations not applying to cloud lightning as they do on controlled environments or applying in such a difficult condition to be observable, perhaps due to unknown effects regarding the behaviour of the electric field along the leader propagation or other possibilities such as a hypothetical balancing between the density and the velocity (thus, the current) of electrons, in such fashion that the reduced electric field (E/n) does not vary as expected, or even the fact that the detected pulse could be the result of more than one streamer emission. This in turn implies that the process regarding VHF emission does not seem to rely, at least directly,on air pressure changes. An equally important fact worthy of mention is that VHF emission is directly proportional to a change in velocity, and not on velocity (i.e. current) itself. Thus what generates current variation in laboratory environments, that is, the mechanism that changes the current on controlled discharges may not be the same one that takes place on natural discharges. These speculations however require further study using different methods.

Another interesting observation is that the amplitude distributions found at the highest amplitudes (where imaging efficiency is constant) shows an approximately linear dependency on a double log-scale. The values for this power, as shown in table 4.1, vary considerably, probably due to poor statistics, but seem to have a mean value of about three. This strongly implies that the amplitude distribution follows a power law, which is scale invariant.

CHAPTER 6

PUBLICATIONS

Formal works used as the basis for the development of this dissertation follow:

- AGU Fall Meeting 2020

The preliminary data analysis and conclusions were presented at the annual AGU international conference [38], the AGU Fall Meeting of 2020, where thanks to rich discussions and questions raised along this work presentation it was possible to further develop the methods used to analyse the data and properly extract the sought information.

URL: `https://agu.confex.com/agu/fm20/meetingapp.cgi/Paper/765131`.

- Journal of Geophysical Research: Earth and Space Science

The final work, including all data analysis, discussion of used methods and interpretation of

found results were submitted to international journal: Journal of Geophysical Research: Earth and Space Science [39]. It was accepted and it is now due to publication.

DOI: http://doi.org/10.1002/essoar.10507863.1

CHAPTER 7

ACKNOWLEDGMENTS

This study was financed in part by the Coordenação de Aperfeiçoamento de Pessoal de Nível Superior – Brasil (CAPES) – Finance Code 001 and by the Fundação de Apoio à Pesquisa do Distrito Federal - FAP/DF. The LOFAR cosmic-ray key science project acknowledges funding from an Advanced Grant of the European Research Council (FP/2007-2013) / ERC Grant Agreement n. 227610. The project has also received funding from the European Research Council (ERC) under the European Union's Horizon 2020 research and innovation programme (grant agreement No 640130). We furthermore acknowledge financial support from FOM, (FOM-project 12PR304). ST acknowledges funding from the Khalifa University Startup grant (project code 8474000237). BMH is supported by NWO (VI.VENI.192.071). KM is supported by FWO (FWO-12ZD920N). AN acknowledges the DFG grant NE 2031/2-1. TNGT acknowledges funding from the Vietnam National Foundation for Science and Technology Development (NAFOSTED) under [Grant number 103.01-2019.378]. LOFAR, the Low Frequency

Array designed and constructed by ASTRON, has facilities in several countries, that are owned by various parties (each with their own funding sources), and that are collectively operated by the International LOFAR Telescope foundation under a joint scientific policy.

The data for the figures can be found at [40]. The raw LOFAR data are available from the LOFAR Long Term Archive (for access see [41]). To download this data, please create an account and follow the instructions for "Staging Transient Buffer Board data" atla [41]. In particular, the utility "wget" should be used as follows:

```
wget https://lofar-download.grid.surfsara.nl/lofigrid/SRMFifoGet.py?surl="location"
```

where "location" should be specified as:

```
srm://srm.grid.sara.nl/pnfs/grid.sara.nl/data/lofar/ops/TBB/lightning/
```

followed by

`L612746\_D20170929T202255.000Z_"stat"_R000_tbb.h5` (for the 2017 Flash),

`D20180813T153001.413Z_"stat"_R000_tbb.h5` (for the 2018 Flash),

and where "stat" should be replaced by the name of the station: CS001, CS002, CS003, CS004, CS005, CS006, CS007, CS011, CS013, CS017, CS021, CS024, CS026, CS028, CS030, CS031, CS032, CS101, CS103, RS106, CS201, RS205, RS208, RS210, CS301, CS302, RS305, RS306, RS307, RS310, CS401, RS406, RS407, RS409, CS501, RS503, RS508, or RS509.

Bibliography

[1] D.J. Malan. *Physics of Lightning*. English Universities Press, 1964.

[2] Feng Shi, Ningyu Liu, Joseph R. Dwyer, and Kevin M. A. Ihaddadene. Vhf and uhf electromagnetic radiation produced by streamers in lightning. *Geophysical Research Letters*, 46(1):443–451, 2019.

[3] Brian M. Hare, O. Scholten, J. Dwyer, U. Ebert, S. Nijdam, A. Bonardi, S. Buitink, A. Corstanje, H. Falcke, T. Huege, J. R. Hörandel, G. K. Krampah, P. Mitra, K. Mulrey, B. Neijzen, A. Nelles, H. Pandya, J. P. Rachen, L. Rossetto, T. N. G. Trinh, S. ter Veen, and T. Winchen. Radio emission reveals inner meter-scale structure of negative lightning leader steps. *Phys. Rev. Lett.*, 124:105101, 2020.

[4] Olaf Scholten et al. Time resolved 3d interferometric imaging of a section of a negative leader with lofar. *Accepted for publication in Phys. Rev. D*, 2021.

[5] O. Scholten, B.M. Hare, J. Dwyer, N. Liu, C. Sterpka, S. Buitink, A. Corstanje, H. Falcke, T. Huege, J.R. Hörandel, G.K. Krampah, P. Mitra, K. Mulrey, A. Nelles, H. Pandya, J.P. Rachen, T.N.G. Trinh, S. ter Veen, S. Thoudam, and T. Winchen. Distinguishing features of high altitude negative leaders as observed with lofar. *Atmospheric Research*, 260:105688, 2021.

[6] J. R. Dwyer and M. A. Uman. The physics of lightning. *Physics Reports*, 534(4):147–241, 2014.

[7] Sander Nijdam, Jannis Teunissen, and Ute Ebert. The physics of streamer discharge phenomena. *Plasma Sources Science and Technology*, 29(10):103001, 2020.

[8] Xuebao Li, Xiang Cui, Tiebing Lu, Dayong Li, Bo Chen, and Yuke Fu. Influence of air pressure on the detailed characteristics of corona current pulse due to positive corona discharge. *Physics of Plasmas*, 23(12):123516, 2016.

[9] Briels T.M.P, E.M. van Veldhuizen, and U. Ebert. Positive streamers in air and nitrogen of varying density: experiments on similarity laws. *Journal of Physics D*, 41:234008, 2008.

[10] T. Huiskamp, A.J.M. Pemen, W.F.L.M. Hoeben, F.J.C.M. Beckers, and E.J.M. van Heesch. Temperature and pressure effects on positive streamers in air. *Journal of Physics D*, 46:165202, 2013.

[11] Vanna C. Chmielewski and Eric C. Bruning. Lightning mapping array flash detection performance with variable receiver thresholds. *Journal of Geophysical Research: Atmospheres*, 121(14):8600–8614, 2016.

[12] R. J. Thomas, P. R. Krehbiel, T. Hamlin W. Rison, J. Harlin, and D. Shown. Observations of vhf source powers radiated by lightning. *Geophysical Research Letters*, 28(1):143–146, 2001.

[13] B. M. Hare, O. Scholten, J. Dwyer, T. N. G. Trinh, S. Buitink, S. ter Veen, A. Bonardi, A. Corstanje, H. Falcke, J. R. Hörandel, T. Huege, P. Mitra, K. Mulrey, A. Nelles, J. P. Rachen, L. Rossetto, P. Schellart, T. Winchen, J. Anderson, I. M. Avruch, M. J. Bentum, R. Blaauw, J. W. Broderick, W. N. Brouw, M. Brüggen, H. R. Butcher, B. Ciardi,

R. A. Fallows, E. de Geus, S. Duscha, J. Eislöffel, M. A. Garrett, J. M. Grießmeier, A. W. Gunst, M. P. van Haarlem, J. W. T. Hessels, M. Hoeft, A. J. van der Horst, M. Iacobelli, L. V. E. Koopmans, A. Krankowski, P. Maat, M. J. Norden, H. Paas, M. Pandey-Pommier, V. N. Pandey, R. Pekal, R. Pizzo, W. Reich, H. Rothkaehl, H. J. A. Röttgering, A. Rowlinson, D. J. Schwarz, A. Shulevski, J. Sluman, O. Smirnov, M. Soida, M. Tagger, M. C. Toribio, A. van Ardenne, R. A. M. J. Wijers, R. J. van Weeren, O. Wucknitz, P. Zarka, and P. Zucca. Needle-like structures discovered on positively charged lightning branches. *Nature*, 568:360–363, 2019.

[14] O. Scholten, B. M. Hare, J. Dwyer, C. Sterpka, I. Kolmasova, O. Santolik, R. Lan, L. Uhlir, S. Buitink, A. Corstanje, H. Falcke, T. Huege, J. R. Hoerandel, G. K. Krampah, P. Mitra, K. Mulrey, A. Nelles, H. Pandya, A. Pel, J. P. Rachen, T. N. G. Trinh, S. ter Veen, S. Thoudam, and T. Winchen. The initial stage of cloud lightning imaged in high-resolution. *Journal of Geophysical Research: Atmospheres*, 126(4):e2020JD033126, 2021.

[15] M. P. van Haarlem et al. Lofar: The low-frequency array. *Astronomy & Astrophysics*, 556(A2), 2013.

[16] B. M. Hare, O. Scholten, A. Bonardi, S. Buitink, A. Corstanje, U. Ebert, et al. Lofar lightning imaging: Mapping lightning with nanosecond precision. *Journal of Geophysical Research: Atmospheres*, 123:2861–2876, 2018.

[17] A. Chilingarian, S. Chilingaryan, T Karapetyan, et al. On the initiation of lightning in thunderclouds. *Scientific Reports, Nature*, 1371, 2017.

[18] V. S Komelkov. Structure and parameters of the leader discharge. *Bulletin of the Academy of Sciences of the USSR*, 8, 1947.

[19] B. F. J. Schonland. The lightning discharge. *Hanbuch der Physik*, 4, 1956.

[20] R. G. Fowler. Lightning. *Applied Atmospheric Collision Physics*, 5, 1982.

[21] C. E. Baum. *Lightning Electromagnetics*, pages 3–16. Hemisphere, 1990.

[22] P. Laroche, A. Castellani, P. Lalande, I. Gallimberti, A. Bondiou-Clergerie, and G.L Bacchiega. Experimental and theoretical study of the bi-leader process. part ii : theoretical investigation. *IEE Proceedings-Science Measurement And Technology*, 145, 1998.

[23] B. N. Gorin, V. I. Levitov, and A.V Shkilev. Some principles of leader discharge of air gaps with a strong non-uniform field. *Gas Discharges, IEEE Conference Publications*, 143, 1976.

[24] V. A. Rakov and M. A Uman. *Lightning: Physics and Effects*. Cambridge University Press, 3rd edition, 2003.

[25] V. Cooray and L. Arevalo. Modeling the stepping process of negative lightning stepped leaders. *Atmosphere*, 8, 12 2017.

[26] Les Renardières Group. Negative discharges in long air gaps at les renardieres. *Electra*, 74, 1981.

[27] L. B. Loeb. *Electrical Coronas*. University of California Press, 1965.

[28] C. T. R. Wilson. The acceleration of beta-particles in strong electric fields such as those of thunder-clouds. *Proceedings of the Cambridge Philosophical Society*, 22, 1925.

[29] V.P. Pasko. Recent advances in theory of transient luminous events. *Journal of Geophysical Research*, 115, 2010.

[30] V. V. Surkov and M. Hayakawa. Underlying mechanisms of transient luminous events: a review. *Annals of Geophysics*, 30, 2012.

[31] V. A. Rakov. Initiation of lightning in thunderclouds. In Alexander M. Sergeev, editor, *Topical Problems of Nonlinear Wave Physics*, volume 5975, pages 362–373. International Society for Optics and Photonics, SPIE, 2006.

[32] C. D. Weidman and E. P. Krider. The radiation fields wave forms produced by intracloud lightning discharge processes. *Journal of Geophysical Research*, 84:3159–3164, 1979.

[33] J. R. Dwyer, D. M .Smith, and S. A. Cummer. High-energy atmospheric physics: Terrestrial gamma-ray flashes and related phenomena. *Space Science Reviews*, 173, 2012.

[34] P O Kochkin, A P J van Deursen, and U Ebert. Experimental study on hard x-rays emitted from metre-scale negative discharges in air. *Journal of Physics D: Applied Physics*, 48(2):025205, 2014.

[35] Sebastien Celestin, Wei Xu, and Victor P. Pasko. Variability in fluence and spectrum of high-energy photon bursts produced by lightning leaders. *Journal of Geophysical Research: Space Physics*, 120(12), 2015.

[36] O. Scholten. *Practical guide to lightning imaging with LOFAR (internal report)*. Kapteyn Institute, University of Groningen, NL, 2020.

[37] A. Nelles, J. R. Hörandel, T. Karskens, M. Krause, S. Buitink, A. Corstanje, et al. Calibrating the absolute amplitude scale for air showers measured at lofar. *Journal of Instrumentation*, 10, 2015.

[38] Machado J.G.O., Scholten O., Hare B.H., and Ferreira I.S. Altitude x amplitude relations on negative leaders produced by lightning data acquired by lofar. In *AGU Fall Meeting*, 2020.

[39] Machado J.G.O. et al. The relationship of lightning radio pulse amplitudes and source altitudes as observed by lofar. *Journal of Geophysical Research: Earth and Space Science*, 2021. Accepted to publication.

[40] Machado J.G.O et al. Processed Data for "The relationship of lightning radio pulse amplitudes and source altitudes as observed by LOFAR", 2021.

[41] ASTRON. LOFAR Long Term Archive Access. `https://www.astron.nl/lofarwiki/doku.php?id=public:lta_howto`, 2020.